CrossMark

Cognitive Impairment and Brain and Peripheral Alterations in a Murine Model of Intraventricular Hemorrhage in the Preterm Newborn

Antonio Segado-Arenas[1] · Carmen Infante-Garcia[2,3] · Isabel Benavente-Fernandez[1] ·
Daniel Sanchez-Sotano[1,2] · Juan Jose Ramos-Rodriguez[2,3] ·
Almudena Alonso-Ojembarrena[1] · Simon Lubian-Lopez[1,4] · Monica Garcia-Alloza[2]

Abstract Germinal matrix hemorrhage-intraventricular hemorrhage (GMH-IVH) remains a serious complication in the preterm newborn. The significant increase of survival rates in extremelye preterm newborns has also contributed to increase the absolute number of patients developing GMH-IVH. However, there are relatively few available animal models to understand the underlying mechanisms and peripheral markers or prognostic tools. In order to further characterize central complications and evolution of GMH-IVH, we injected collagenase intraventricularly to P7 CD1 mice and assessed them in the short (P14) and the long term (P70). Early complications at P14 included ventricle enlargement, increased bleeding, and inflammation. These alterations were maintained at P70, when increased tau phosphorylation and decreased neurogenesis were also observed, resulting in impaired learning and memory in these early adult mice. We additionally analyzed peripheral blood biomarkers in both our mouse model and preterm newborns with GMH-IVH. While MMP9 levels were not significantly altered in mice or newborns, reduced gelsolin levels and increased ubiquitin carboxy-terminal hydrolase L1 and tau levels were detected in GMH-IVH patients at birth. A similar profile was observed in our mouse model after hemorrhage. Interestingly, early changes in gelsolin and carboxy-terminal hydrolase L1 levels significantly correlated with the hemorrhage grade in newborns. Altogether, our data support the utility of this animal model to reproduce the central complications and peripheral changes observed in the clinic, and support the consideration of gelsolin, carboxy-terminal hydrolase L1, and tau as feasible biomarkers to predict the development of GMH-IVH.

Keywords Germinal matrix hemorrhage-intraventricular hemorrhage · Neurogenesis · Tau · Gelsolin · Carboxy-terminal hydrolase L1

✉ Simon Lubian-Lopez
   simonp.lubian.sspa@juntadeandalucia.es

✉ Monica Garcia-Alloza
   monica.garcia@uca.es

[1] Division of Neonatology, Hospital Universitario Puerta del Mar, Cadiz, Spain

[2] Division of Physiology, School of Medicine, Instituto de Investigación Biomédica e Innovación en Ciencias Biomédicas de la Provincia de Cádiz (INiBICA), Universidad de Cadiz, Plaza Fragela sn, 4 piso 410, Cadiz, Spain

[3] Salus Infirmorum, Universidad de Cadiz, Cadiz, Spain

[4] Division of Pediatrics, Hospital Universitario Puerta del Mar, Ava. Ana de Villa sn, Cadiz, Spain

Introduction

Germinal matrix-intraventricular hemorrhage (GMH-IVH) remains a serious problem in the preterm newborn (PTNB). Despite the improvement of neonatal critical care in the last decades, the absolute number of infants who develop severe GMH-IVH has not declined, mostly due to a significant increase of the survival rates of the very and extremely preterm infant (for review [1]). GMH-IVH results from bleeding from the germinal matrix, a complex vascularized layer also corresponds with the subventricular zone (SVZ), from where neurons and glial cells rise during fetal development [2]. Germinal matrix starts to involute by 28 weeks of gestational age, and it is generally absent in term newborns, while the PTNB are susceptible to local hemorrhage due to the extreme friability of these capillaries, combined with their inability to autoregulate cerebral blood flow [2]. While GMH-IVH can

 Springer

occur a few days later, it has been reported that ~80% of all cases occur within the first 72 h after birth. GMH-IVH can expand in the following day, leading to adjacent parenchymal involvement and the development of ventriculomegaly [3].

The short- and long-term neurodevelopmental outcomes in infants with severe GMH-IVH are a major concern, as GMH-IVH increases the risk of cerebral palsy and neurodevelopmental or psychomotor alterations [4, 5]. Even mild GMH-IVH has been associated with major neurological abnormalities and neurodevelopmental impairment in preterm infants [6, 7]. Whereas the relevance of these consequences is out of question, there is no consensus regarding timing of intervention, markers, predictors, or treatment [8]. Therefore, controllable and reproducible animal models of GMH-IVH are essential to study feasible markers, therapies, and preventive measures [9]. In this regard, diverse options have been explored with variable success, including physiologic manipulations (hyperosmolar or hypertensive agents, induction of hypoxia, hypercapnia, or hypervolemia) or injections of donor or autologous blood into the periventricular region (for review [10]). On the other hand, intraventricular administration of collagenase might provide a simple and reproducible method to induce GMH-IVH, as previously shown in rats [9]. Collagenases are proteolytic intracellular enzymes that hydrolyze collagen, a major component of the basal lamina of blood vessels. Therefore, direct injection of collagenase dissolves the extracellular matrix surrounding capillaries, opens the blood-brain barrier, and induces intracranial bleeding [9]. To our knowledge, this approach has not been used in mice, and long-term (up to early adulthood) morphopathological and behavioral changes have not been addressed. Moreover, feasible markers have not been explored, and observations have not been correlated to outcomes in PTNB patients with GMH-IVH. We have found that induction of GMH-IVH to newborn mice results in early central bleeding, brain atrophy, neuronal loss, impaired neurogenesis, and inflammation. These alterations, as well as increased tau hyperphosphorylation as a marker of neuronal damage, and behavioral impairments are observed up to the early adulthood in collagenase-treated mice. Exploring peripheral feasible markers of GMH-IVH complications revealed that while matrix-metalloproteinase 9 (MMP9) was not altered, ubiquitin carboxy-terminal hydrolase L1 (UCH-L1), gelsolin, and tau levels were significantly affected early on in our animal model. Moreover, PTNB with GMH-IVH exhibited a similar profile of changes in UCH-L1, gelsolin, and tau levels at birth. Interestingly, early changes in UCH-L1 and gelsolin were significantly correlated with hemorrhage severity grade in PTNB patients. Altogether, our mouse model mimics morphopathological and functional changes observed in GMH-IVH patients in the short and the long term, allowing for therapeutic alternatives in a chronic neuropathological situation to be developed. Additionally, are similar, in both our animal model and human samples,

indicates the power of such an animal model and allows for future exploration of serum UCH-L1, gelsolin, or tau as possible predictors of GMH-IVH severity in PTNB patients.

Material and Methods

Animals and Treatments

Male and female CD1 offspring underwent a lesion by a collagenase VII (Col) (Sigma, St. Louis, MO) intracerebroventricular (icv) infusion at P7, as previously described with minor modifications [11]. Briefly, mice were anesthetized with isoflurane and immobilized in a stereotactic frame (David-Kopf, CA, USA); 0.1 or 0.3 IU of Col in 1 μl of TESCA was administered in the right ventricle (AP −3 mm, ML −1 mm, and DV +4 mm, using bregma as a reference) at 0.2 μl/min, using a Hamilton syringe, which was left in the lesion site for five more minutes after completing the administration process. Sham animals underwent the same surgical approach but received 1 μl PBS. Newborn mice were allowed to recover and returned to the cage with their mothers. All animals were weighted before the lesions and before sacrifice, at P14 or P70. For proliferation and neurogenesis studies, animals received ip 5-bromo-3-deoxyuridine (BrdU; 70 mg/kg) for three consecutive days before sacrifice. All experimental procedures were approved by Junta de Andalucia (Guidelines for Care and Use of Experimental Animals, European Commission Directive 2010/63/UE and Spanish Royal Decree 53/2013) and the University of Cadiz Bioethical Committee.

Rotarod

Motor skills were evaluated in the rotarod (Ugo Basile Srl; Varese, Italia) as previously described with minor modifications [12]. Animals were placed on the apparatus for 3 min at 4 rpm for habituation purposes. During the test probe, the speed was increased from 4 to 60 rpm within 1 min, and the time spent on the rotarod was recorded.

New Object Discrimination Task

Seven days prior to sacrifice at P70, episodic memory was assessed as previously described [13]. For the purpose of habituation, mice were exposed to two objects in a transparent rectangular box (22 cm long × 44 cm width × 40 cm high), which were not used again during the object exploration task. The next day, each mouse underwent two sample trials and a test trial. On the first sample trial, mice were placed in the center of a box containing four copies of a novel object (blue balls) arranged in a triangle-shaped spatial configuration and were allowed to explore

them for 5 min. After a delay of 30 min, the mice underwent a second sample trial with four novel objects (red cones), arranged in a quadratic-shaped spatial configuration, for 5 min. After a delay of 30 min, the mice went through a test trial with two copies of the object from sample trial no. 2 (recent objects) placed in the same position, and two copies of the object from sample trial no. 1 (familiar objects): one of them in the same position (familiar nondisplaced object) and the other one in a new position (familiar displaced object). Integrated episodic memory for "what," "where," and "when" was analyzed as previously described [13] using SMART system (Panlab, Spain).

Morris Water Maze

The day after concluding the new object discrimination (NOD) test, mice were subjected to the Morris water maze (MWM) task as previously described [13]. Briefly, the maze consisted of a round tank of water (0.95 m in diameter) with four equal virtual quadrants indicated with geometric cues mounted on the walls. An escape platform was located 2–3 cm below the water surface and camouflaged with calcium carbonate to cloud the water. Water temperature was 21 ± 1 °C. A camera was mounted above the maze and attached to a computer and SMART software (Panlab, Spain). Acquisition consisted of 4 trials/day for 4 days with the platform submerged. During this phase, the platform was placed in quadrant 2. The time limit was 60 s/trial with an intertrial interval of 10 min. If the mouse did not find the platform, the mouse was placed on it for 10 s. The retention phase took place 24 h (retention no. 1) and 72 h (retention no. 2) after the acquisition phase. In this phase, the submerged platform was removed, mice were allowed to swim for 60 s, and the time mice spent in the quadrant where the platform was previously located (quadrant 2) was recorded using SMART system (Panlab, Spain). Swimming velocity was also measured in order to detect any motor activity dysfunction that could interfere with cognitive assessment.

Tissue Processing

Brains were harvested and weighed (P14 and P70). Blood samples (~700 μl) were collected in heparinized tubes, and after centrifuging for 10 min (6500 rpm), plasma was frozen at −80 °C until used. The ipsi- and contralateral cortex, hippocampus, and striatum were dissected in half of the animals and snap frozen for caspase activity and western blot studies. The brains from the remaining animals were fixed in paraformaldehyde for 2 weeks and 30-μm-thick coronal sections were obtained for staining and immunostaining procedures.

Cresyl Violet Staining

Brain morphology was analyzed after cresyl violet staining in sections 0.5 mm apart (from 1.0 to −1.0 mm from bregma). Sections were mounted and dehydrated in 70% ethanol for 15 min before being incubated in cresyl violet (Sigma, St. Louis, MO, USA) solution 0.5% (w/v) for 5 min. Sections were washed and fixed in 0.25% acetic acid in ethanol for 7 min and subsequently in 100% ethanol and xylene for 2 min. Sections were mounted with DPX (Sigma, St. Louis, MO, USA) and photographed with a Laser Olympus U-RFLT fluorescent microscope (Olympus, Japan). Images were acquired using MMIcellTools software. Hemisection and ventricle sizes were measured using ImageJ software.

Prussian Blue Staining

Hemorrhages were detected using Prussian blue iron staining and neutral red counterstain in consecutive sections to those used for cresyl violet staining. Sections were mounted on slides and exposed to Prussian blue staining (10% HCl and 5% potassium ferrocyanide) for 30 min and then rehydrated with PBS for 10 min. Sections were dehydrated in 70% alcohol and immersed in a neutral red solution 1% (v/w) for 5 min. After washing, sections were fixed in 95% ethanol (with 1% acetic acid) and immersed in xylol for 4 min. Sections were mounted with DPX (Sigma, St. Louis, MO, USA) and imaged with an Olympus Bx60 microscope (Japan) equipped with an Olympus DP71 camera. Images were analyzed using Adobe PhotoShop and ImageJ software to quantify hemorrhage burden in the cortex, striatum, and hippocampus [14].

Immunohistochemistry Studies: 5-Bromo-3-deoxyuridin, Doublecortin, NeuN, and Microglia

BrdU and doublecortin (DCX) immunohistochemistry was performed in the SVZ, the subgranular zone of the dentate gyrus (DG), the cortex, and the hippocampus. Anti-BrdU 1:100 (Dako, Barcelona, Spain) and anti-DCX 1:400 (Santa Cruz Biotechnology, Santa Cruz, CA, USA) were used as primary antibodies, and Alexa Fluor 594 and Alexa Fluor 488 (1:100) (Invitrogen, Carlsbad, CA, USA) as secondary antibodies [14]. DCX burden (percentage of area covered by DCX-positive cells) was quantified in the SVZ [14], and the number of individual DCX- and BrdU-positive cells was quantified in the DG, cortex, and hippocampus using ImageJ software.

NeuN and microglia immunohistochemistry was performed as described [15]. Anti-Iba1 (Wako, Osaka, Japan) (1:2000) or anti-NeuN (Chemicon, CA, USA) (1:200) (Invitrogen, Carlsbad, CA, USA) were used as primary antibodies to mark microglia and neurons respectively. Alexa Fluor 488 and Alexa Fluor 594 (1:200) as secondary antibodies. DAPI 1 mg/ml (Sigma)

(1:2000) counterstain was used. The percentage of NeuN-positive cells (normalized by total cells stained with DAPI) was quantified as previously described [16] in the SVZ, cortex, and hippocampus. Microglia burden was also quantified in the SVZ, cortex, and hippocampus using ImageJ software as previously described [17].

Western Blot for Total Tau and Phospho-Tau Levels

Western blots for phospho-tau and total tau levels were performed in fresh tissue as previously described [18]. Briefly, 50 μg of protein from the cortex, hippocampus, and striatum was loaded and separated on 10% acrylamide-bisacrylamide gels. Proteins were transferred to PVDF membranes and then immersed in blocking buffer (Invitrogen) for 1 h prior to overnight incubation at 4 °C with primary antibodies: anti-phospho-tau (1:1000, clone AT8; Fisher Scientific, Waltham, MA), anti-total tau (1:1000; DAKO, Glostrup, Denmark), and anti-β-actin (1:2.500, Sigma, USA). Signal was detected using Novex AP Chemiluminescent Substrate (Invitrogen, Carlsbad, USA) and Kodak Biomax Light Film (Sigma, USA). Subsequent incubations of primary antibodies were preceded by stripping, using western blot stripping buffer (Fisher Scientific, Waltham, MA). Optical density of each protein band was quantified using the ImageJ software. Data were represented as percentage of control values.

Patients and Samples

Plasma samples obtained from PTNB patients from the Neonatal Intensive Care Unit (NICU) of the Puerta del Mar University Hospital between 2015 and 2016 were included in the study. Plasma samples were collected at birth and on day 7 after birth. All studies were approved by the Hospital Bioethics Committee in accordance with the Declaration of Helsinki and Spanish law on Biomedical Research 14/2007 and Data Protection 15/1999.

Inclusion criteria were PTNB <32 gestational weeks and/or <1500 g body weight who required admission to the NICU, confirmation of GMH-IVH by transcranial ultrasound within 7 days, and written informed consent to participate in the study signed by parents or legal guardians. Exclusion criteria were chromosomopathies, congenital malformations, early onset sepsis caused by vertical transmission or congenital infection confirmed by microbiological studies, or death within the first 24 h of life.

PTNB patients were classified into control ($n = 10$) and GMH-IVH groups ($n = 16$; hemorrhage grade 1, $n = 3$; grade 2, $n = 8$; grade 3, $n = 1$; and grade 4, $n = 4$). Hemorrhage was classified following Volpe's classification [19]. Variables recorded included gender, gestational age, birth weight, Apgar 1 and Apgar 5 scores, cesarean section, systolic and diastolic blood pressures at admission to the NICU, Score for Neonatal Acute Physiology Perinatal Extension (SNAPPE-II), Clinical Risk Index for Babies (CRIB) score, need for mechanical ventilation in the first 24 h, and need for inotropic support in the first 24 h (Table 1).

Plasma Biomarkers: Tau, UCH-L1, Gelsolin, and MMP9

Plasma samples from mice and PTNB patients were processed with the following ELISA kits according to the manufacturer's instructions: tau (mouse and human: Abcam, UK), UCH-L1 (mouse and human: Biosource, CA, USA), gelsolin (mouse: Cusabio Biotech Co, China; human: Abiscera Bioscience, CA, USA), and MMP9 (mouse and human: R&D System Corp, MN, USA).

Statistical Analyses

Student's t test for independent samples or one-way ANOVA, followed by Tukey b or Tamhane tests, as required, was used. Since no statistical differences were detected between sham and control groups, sham and control animals were combined in a single control group. Two-way ANOVA tests (group × day) were used to analyze the MWM test. Pearson's or Spearman's rank correlation tests were used to correlate peripheral biomarkers with central alterations and cognitive impairment in animals and medical history data in PTNB patients. SPSS v.15 software was used for all statistical analyses.

Results

GMH-IVH Causes Long-Term Learning and Memory Disabilities

Learning impairment was observed in the NOD test for the Col 0.1 group, and a decline in learning abilities was detected for the Col 0.3 group when animals were assessed in the early adulthood (~2.5 months old). Data are representative of 9–14 mice, and since no differences were observed between sham and control groups, all these mice were combined in a single control group. A dose-dependent episodic memory impairment was observed under all paradigms studied: what [$F_{(2, 130)} = 109.40,$ **$p < 0.01$ vs. the rest of the groups, ††$p < 0.01$ vs. control], where [$F_{(2, 122)} = 69.84$, **$p < 0.01$ vs. the rest of the groups, ††$p < 0.001$ vs. control], and when [$F_{(2, 130)} = 30.56$, ††$p < 0.001$ vs. control] (Fig. 1a).

A similar profile was observed in the MWM test, with a significant learning impairment in the acquisition phase for the Col 0.1 group and a slight decline in the Col 0.3 group. Data are representative of 9–14 mice, and again, since no differences were observed between sham and control groups, all these mice were combined in a single control group. A

**Table 1** Perinatal and clinical characteristics of infants

	IVH ($n = 10$)	No IVH ($n = 10$)	Total ($n = 26$)
Gestational age (weeks)	27.56 ± 2.2	29.6 ± 1.5	28.35 ± 2.2
Gender (% boys)	6 (37.5%)	6 (60%)	12 (46.15%)
Birth weight (g)	999.38 ± 289.8	1247.5 ± 173.7	1094.81 ± 276.4
Cesarean section	6 (37.5%)	4 (40%)	10 (38.46%)
Apgar 1	5 (2–7)	7 (5–9)	6 (2–9)
Apgar 5	7 (4–8)	8 (7–10)	7 (4–10)
CRIB	2 (0–9)	1 (0–2)	1 (0–9)
SNAPPE-II	32.5 (8–76)	8 (0–17)	18 (0–76)
Systolic pressure (mmHg)	45.44 ± 14.3	49.6 ± 8.8	47.04 ± 12.5
Diastolic pressure (mmHg)	22.19 ± 7.8	28.10 ± 8.2	24.46 ± 8.3
Mechanical ventilation (%)	16 (100%)	6 (60%)	22 (84.61%)
Ionotropic drug use (%)	4 (25%)	1 (10%)	5 (19.23%)

CRIB Clinical Risk Index for Babies, *SNAPPE-II* Score for Neonatal Acute Physiology Perinatal Extension

significant day × treatment effect was observed along the acquisition phase by two-way ANOVA for independent samples [$F_{(6, 645)} = 2.77$, *$p = 0.011$]. Further differences were detected for individual days by one-way ANOVA for independent samples followed by Tukey *b* or Tamhane tests: day 1 [$F_{(2, 181)} = 0.904$, $p = 0.407$], day 2 [$F_{(2, 176)} = 18.78$, ††$p < 0.001$ vs. control], day 3 [$F_{(2, 160)} = 13.7$, ††$p < 0.001$ vs. control], and day 4 [$F_{(2, 171)} = 14.14$, **$p < 0.01$ vs. the rest of the

Fig. 1 Collagenase-induced GMH-IVH provokes dose-dependent cognitive deficits in the long term. **a** Episodic memory was affected in all paradigms under study: what (**$p < 0.01$ vs. the rest of the groups, ††$p < 0.01$ vs. control), where (**$p < 0.01$ vs. the rest of the groups, ††$p < 0.001$ vs. control), and when (††$p < 0.001$ vs. control). **b** A similar profile was observed when spatial memory was assessed in the acquisition phase of the MWM test at P70: day 1 ($p = 0.407$), day 2 (††$p < 0.001$ vs. control), day 3 (††$p < 0.001$ vs. control), and day 4 (**$p < 0.01$ vs. the rest of the groups, ††$p < 0.001$ vs. control). **c** The retention phase in the MWM test also revealed a significant impairment in collagenase-treated mice (24 h: *$p < 0.29$ vs. control group and 72 h: *$p = 0.02$ vs. control group)
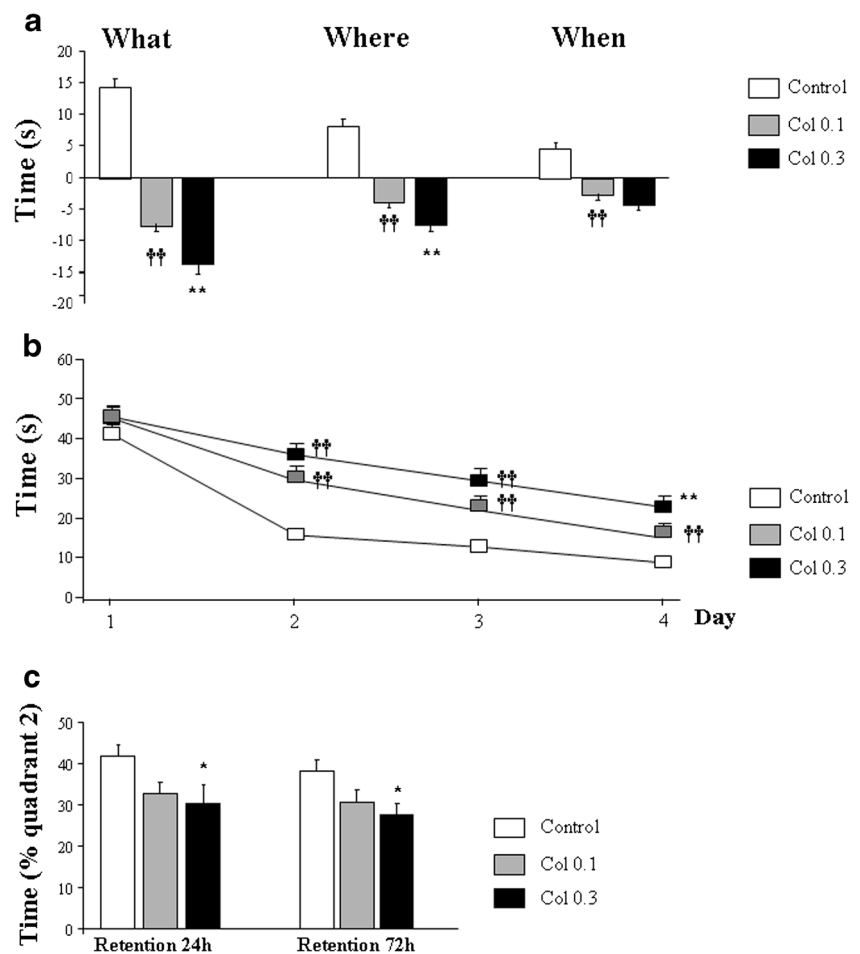
groups, ††$p < 0.001$ vs. control] (Fig. 1b). The retention phase in the MWM test also revealed a significant impairment in collagenase-treated mice, in a dose-dependent manner, which was evident both 24 h [$F_{(2, 35)} = 3.91$, *$p < 0.29$ vs. control group] and 72 h [$F_{(2, 42)} = 4.27$, *$p = 0.02$ vs. control group] after completing the acquisition phase (Fig. 1c). We did not detect significant differences in motor activity, as indicated by the time on the rotarod (control, 12.21 ± 1.20; Col 0.1, 9.93 ± 1.19; 11.83 ± 0.99 s) and the swimming speed in the MWM (control, 26.74 ± 0.98; Col 0.1, 26.54 ± 0.81; 24.55 ± 0.66 cm/s) ([$F_{(2, 42)} = 1.032$, $p = 0.280$] and [$F_{(2, 43)} = 1.58$, $p = 0.217$], respectively).

GMH-IVH Causes Short- and Long-Term Atrophy and Neuronal Loss

Brain weight was assessed at P14 and P70. While we did not detect any significant differences in the short term, 7 days after the lesions (P14 [$F_{(2, 36)} = 0.076$, $p = 0.927$]), in the long term, a significant reduction of brain weight was observed in animals with severe lesions [$F_{(2, 38)} = 4.65$, *$p = 0.016$ vs. the rest of the groups] (Fig. 2a). The fact that body weight was similar in all groups under study suggests that our observations at the central level are not due to differences in animal size (P14 control, 7.96 ± 0.31 g; Col 0.1, 8.78 ± 0.39 g; Col 0.3, 8.61 ± 0.47 g [$F_{(2, 38)} = 1.43$, $p = 0.251$]; P70 control, 29.08 ± 2.43 g; Col 0.1, 29.63 ± 0.67 g; Col 0.3, 33.12 ± 1.65 g [$F_{(2, 43)} = 1.049$, $p = 0.359$]). Further assessment of brain morphology with cresyl violet staining supported macroscopic observations. An overall reduction of the ipsilateral hemisection size was observed at P14 in lesioned animals, although differences only reached statistical significance at 0.5 mm from bregma (1 mm [$F_{(2, 12)} = 0.48$, $p = 0.77$], 0.5 mm [$F_{(2, 13)} = 0.41$, *$p = 0.034$ vs. control], 0.0 mm [$F_{(2, 13)} = 1.81$, $p = 0.202$], −0.5 mm [$F_{(2, 12)} = 3.65$, $p = 0.058$], −1.0 mm [$F_{(2, 8)} = 0.73$, $p = 0.510$]) (Fig. 2b). In the long term (P70), significant brain atrophy was observed in the ipsilateral hemisphere of 0.3 Col-treated mice (1 mm [$F_{(2, 23)} = 10.98$, **$p < 0.01$ vs. the rest of the groups], 0.5 mm [$F_{(2, 25)} = 2.32$, $p = 0.119$], 0.0 mm [$F_{(2, 27)} = 7.13$, **$p = 0.003$ vs. the rest of the groups], −0.5 mm [$F_{(2, 25)} = 2.32$, $p = 0.119$], −1.0 mm [$F_{(2, 19)} = 1.61$, $p = 0.225$]) (Fig. 2b). Brain atrophy was accompanied by ventricle enlargement. We observed that ipsilateral ventricles were slightly enlarged in Col 0.3-treated mice 1 week after the lesion (P14) (1 mm [$F_{(2, 12)} = 3.095$, $p = 0.085$], 0.5 mm [$F_{(2, 13)} = 2.02$, $p = 0.819$], 0.0 mm [$F_{(2, 13)} = 7.19$, **$p = 0.08$ vs. control and Col 0.1], −0.5 mm [$F_{(2, 13)} = 42.51$, $p = 0.119$], −1.0 mm [$F_{(2, 7)} = 8.79$, *$p = 0.012$ vs. control and Col 0.1]) (Fig. 2c, d). Ventricle enlargement was increased in the long term, at P70, and this effect reached statistical significance in animals that received Col 0.3 (1 mm [$F_{(2, 27)} = 3.64$, *$p = 0.04$ vs. control group], 0.5 mm [$F_{(2, 25)} = 1.97$, $p = 0.160$], 0.0 mm [$F_{(2, 27)} = 3.65$, *$p = 0.04$

vs. control group], −0.5 mm [$F_{(2, 25)} = 4.35$, *$p = 0.024$ vs. control group], −1.0 mm [$F_{(2, 24)} = 2.83$, $p = 0.079$]) (Fig. 2e, f). We also analyzed neuronal number and detected a significant compromise 7 days after the lesions. The percentage of neurons was reduced in the ipsilateral SVZ 7 days after the induction of an GMH-IVH, at P14 [$F_{(2, 1466)} = 145.27$, ††$p < 0.01$ vs. control] (Fig. 2g, h). A reduction in the neuronal ratio was also detected in the cortex in the short term [$F_{(2, 281)} = 31.97$, ††$p < 0.01$ vs. control] (Fig. 2g). In the long term, at P70, we observed a similar profile with the neuronal ratio significantly reduced in the SVZ [$F_{(2, 280)} = 59.81$, ††$p < 0.01$ vs. control] (Fig. 2g, h) and the cortex [$F_{(2, 1472)} = 299.34$, ††$p < 0.01$ vs. control] (Fig. 2g).

GMH-IVH Affects Proliferation and Neurogenesis in the Long Term

We analyzed proliferation and neurogenesis in neurogenic niches, SVZ and DG of the hippocampus after GMH-IVH. We did not detect any significant differences in BrdU staining when we analyzed the ipsi- or contralateral SVZ after collagenase injections ([$F_{(2, 47)} = 0.37$, $p = 0.691$] and [$F_{(2, 49)} = 0.76$, $p = 0.473$], respectively) (Fig. 3a, b). However, the area covered by DCX+ cells was significantly reduced in the ipsilateral hemisphere when a 0.3-IU dose of collagenase was used ([$F_{(2, 44)} = 3.73$, *$p = 0.032$ vs. control and Col 0.1 IU], whereas the contralateral hemisphere was not affected [$F_{(2, 48)} = 0.71$, $p = 0.491$]). Similarly, the DCX+ area/number of BrdU+ cells showed a significant reduction in the ipsilateral hemisphere after 0.3 IU collagenase injections ([$F_{(2, 43)} = 15.96$, **$p = 0.005$ vs. control and Col 0.1] and contralateral hemisphere [$F_{(2, 48)} = 1.42$, $p = 0.251$]) (Fig. 3a, b). Number of BrdU+ cells in the DG was maintained at P70, both in the ipsilateral and contralateral hemispheres ([$F_{(2, 30)} = 0.62$, $p = 0.940$] and [$F_{(2, 33)} = 0.450$, $p = 0.641$], respectively). A slight reduction in DCX+ cells was observed in the ipsilateral DG although differences did not reach statistical significance, while the contralateral DG was not affected (ipsilateral [$F_{(2, 32)} = 0.006$, $p = 0.994$], contralateral [$F_{(2, 32)} = 0.519$, $p = 0.600$]). However, the percentage of DCX+/BrdU+ cells was significantly reduced in the ipsilateral DG [$F_{(2, 31)} = 3.82$, †$p = 0.033$ vs. control], while no differences were observed in the contralateral DG [$F_{(2, 30)} = 0.75$, $p = 0.470$] (Fig. 3c, d). We also analyzed BrdU+ and DCX+ cells in the cortex and hippocampus, as relevant regions in learning and memory. The number of BrdU+ cells in the cortex was reduced at P70, after collagenase lesions, both in the ipsilateral and contralateral hemispheres, and differences reached statistical significance in animals injected 0.3 IU (ipsilateral [$F_{(2, 120)} = 3.21$, †$p = 0.04$ vs. control], contralateral [$F_{(2, 120)} = 4.01$, *$p = 0.021$ vs. control]). A similar profile was observed when we quantified DCX+ cells, which were reduced after lesion in both hemispheres, reaching statistical significance at the highest dose of Col in the ipsilateral side ([$F_{(2,}$
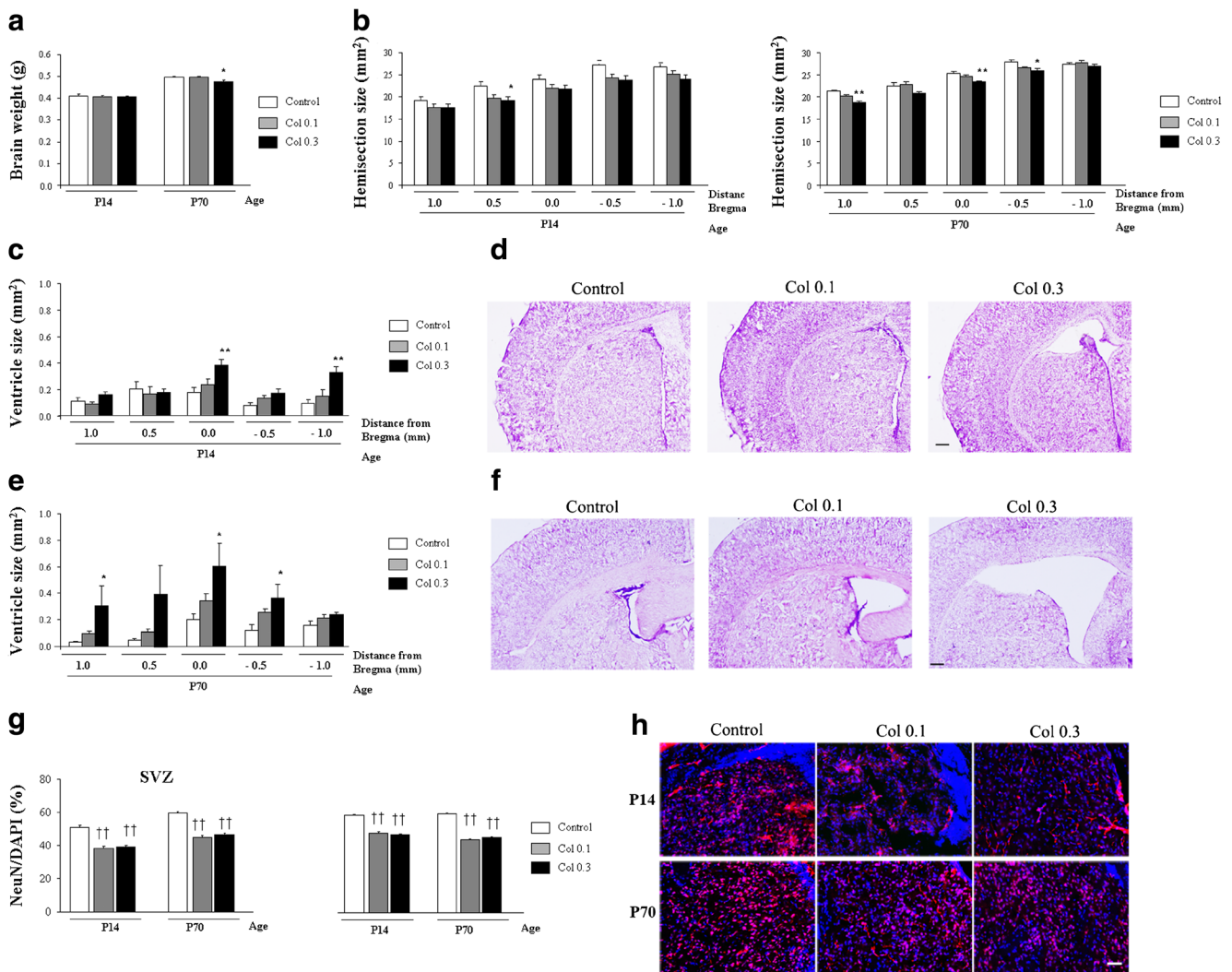
Fig. 2 Brain atrophy and ventricle enlargement is observed in the short and the long term after GMH-IVH. **a** Brain weight was not affected at P14 ($p = 0.927$), whereas a significant reduction was observed at P70 in Col 0.3 (*$p = 0.016$ vs. the rest of the groups). **b** Ipsilateral hemisection size was slightly reduced at P14, although differences only reached statistical significance at 0.5 mm from bregma (1 mm: $p = 0.77$, 0.5 mm: *$p = 0.034$ vs. control, 0.0 mm: $p = 0.202$, −0.5 mm: $p = 0.058$, −1.0 mm: $p = 0.510$). At P70, significant brain atrophy was observed in the ipsilateral hemisphere of 0.3 Col-treated mice (1 mm: **$p < 0.01$ vs. the rest of the groups, 0.5 mm: $p = 0.119$, 0.0 mm: **$p = 0.003$ vs. the rest of the groups, −0.5 mm: $p = 0.119$, −1.0 mm: $p = 0.225$). **c** Ipsilateral ventricles were slightly enlarged in Col 0.3-treated mice at P14 (1 mm: $p = 0.085$, 0.5 mm: $p = 0.819$, 0.0 mm: **$p = 0.08$ vs. control and Col 0.1, −0.5 mm: $p = 0.119$, −1.0 mm:, *$p = 0.012$ vs. control and Col 0.1). **d** Illustrative

example of coronal sections stained with cresyl violet, where ventricle enlargement can be observed in lesioned mice at P14. *Scale bar* = 250 μm. **e** Ventricle enlargement was increased in the long term, at P70 (1 mm: *$p = 0.04$ vs. control group, 0.5 mm: $p = 0.160$, 0.0 mm: *$p = 0.04$ vs. control group, −0.5 mm: *$p = 0.024$ vs. control group, −1.0 mm: $p = 0.079$). **f** Illustrative example where ventricle enlargement can be observed in mice lesioned with collagenase in a dose-dependent manner at P70. *Scale bar* = 250 μm. **g** Neuronal ratio was compromised in the SVZ both at P14 and P70 (††$p < 0.01$ vs. control) and a similar profile was observed in the cortex in the short and the long term (††$p < 0.01$ vs. control). **h** Illustrative example of ipsilateral SVZ after NeuN (*red*) and DAPI (*blue*) staining where a reduction in the number of neurons can be observed in collagenase-treated animals both at P14 and P70. *Scale bar* = 50 μm

$_{123)} = 4.53$, †$p = 0.015$ vs. control] and $[F_{(2, 104)} = 1.54, p = 0.219$ vs. control], respectively). The percentage of DCX+/BrdU+ cells was also reduced in collagenase-lesioned animals, although differences only reached statistical significance in the ipsilateral hemisphere ($[F_{(2, 114)} = 3.98$, †$p = 0.021$ vs. control] and contralateral $[F_{(2, 102)} = 0.806, p = 0.449$ vs. control], respectively) (Fig. 3e). Number of BrdU-positive cells in the hippocampus was also reduced after Col lesions, both in the

ipsilateral and contralateral hemispheres, and differences reached statistical significance after 0.3 IU lesions (ipsilateral $[F_{(2, 58)} = 4.10$, †$p = 0.021$ vs. control], contralateral $[F_{(2, 58)} = 3.25$, †$p = 0.046$ vs. control]). DCX+ cells were also reduced after the lesion in both hemispheres, reaching statistical significance at the highest dose (ipsilateral $[F_{(2, 58)} = 4.10$, †$p = 0.021$ vs. control], contralateral $[F_{(2, 58)} = 3.25$, †$p = 0.046$ vs. control]). The ratio of DCX+/BrdU+ cells was
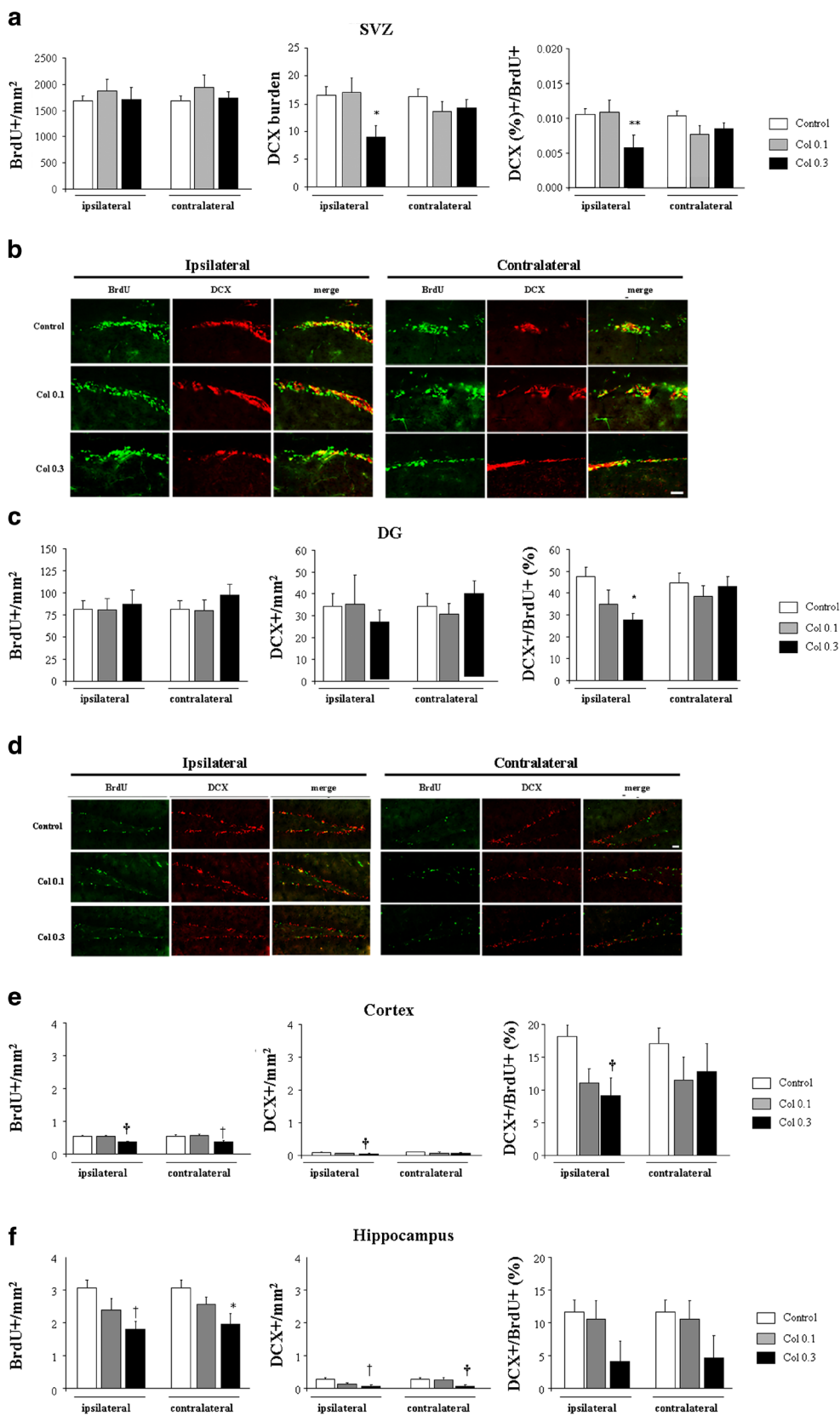
also reduced in collagenase-lesioned animals, although the differences were not statistically significant (ipsilateral [$F_{(2, 49)}$ = 1.22, $p = 0.334$ vs. control], contralateral [$F_{(2, 50)}$ = 2.42, $p = 0.099$ vs. control]) (Fig. 3f).

◄ **Fig. 3** Proliferation and neurogenesis are impaired after GMH-IVH induction. **a** BrdU-positive cells were not affected in the SVZ after collagenase injections (ipsilateral $p = 0.691$ and contralateral $p = 0.473$). However, DCX burden was significantly reduced in the ipsilateral in the Col 0.3 group (*$p = 0.032$ vs. control and Col 0.1 IU), whereas the contralateral hemisphere was not affected ($p = 0.491$). DCX burden/ number of BrdU cells was also reduced in the ipsilateral hemisphere (**$p = 0.005$ vs. control and Col 0.1) and unaffected in the contralateral hemisphere ($p = 0.251$). **b** Illustrative image of the SVZ where reduced DCX burden can be observed in the ipsilateral Col 0.3 group. *Scale bar* = 40 μm. **c** BrdU-positive cells were not affected in the DG (ipsilateral $p = 0.940$, contralateral $p = 0.641$). DCX+ cells were slightly reduced in the ipsilateral hemisphere although differences did not reach statistical significance (ipsilateral $p = 0.994$, contralateral $p = 0.600$). However, the percentage of DCX+/BrdU+ cells was significantly reduced in the ipsilateral DG (†$p = 0.033$ vs. control) without affecting the contralateral DG ($p = 0.470$). **d** Illustrative image of the DG from all groups under study where reduced DCX+/BrdU+ can be observed in the Col 0.3 group. *Scale bar* = 40 μm. **e** BrdU-positive cells were reduced in the ipsi- and contralateral cortices in the Col 0.3 group (ipsilateral †$p = 0.04$ vs. control, contralateral *$p = 0.021$ vs. control). A similar profile is observed when we quantified DCX-positive cells (ipsilateral †$p = 0.015$ vs. control, contralateral $p = 0.219$ vs. control). The percentage of DCX-positive/BrdU-positive cells was also reduced in Col 0.3-lesioned animals (ipsilateral †$p = 0.021$ vs. control, contralateral $p = 0.449$ vs. control). **f** BrdU-positive cells were reduced in the hippocampus from the Col 0.3 group (ipsilateral †$p = 0.021$ vs. control, contralateral †$p = 0.046$ vs. control). DCX-positive cells were also reduced after the lesion in both hemispheres (ipsilateral †$p = 0.021$ vs. control, contralateral †$p = 0.046$ vs. control). The percentage of DCX-positive/BrdU-positive cells was also reduced in collagenase-lesioned animals, although differences did not reach statistical significance (ipsilateral $p = 0.334$ vs. control, contralateral $p = 0.099$ vs. control)

Collagenase-Induced GMH-IVH Leads to Widespread Bleeding in the Brain

We analyzed hemorrhages in areas close to the injection site as well as in remote regions, both in the short and the long term. When we analyzed the striatum at P14, collagenase injections increased hemorrhage burden, reaching statistical significance in the Col 0.3 group [$F_{(2, 55)} = 3.25$, †$p = 0.046$ vs. control]. This effect was maintained in P70 mice, in which the hemorrhage burden was increased in a dose-dependent manner in the Col 0.1 and Col 0.3 groups [$F_{(2, 55)} = 22.99$, **$p < 0.01$ vs. the rest of the groups, ††$p < 0.01$ vs. control] (Fig. 4a, d). The hippocampus was affected in a similar way, and bleeding was increased in a dose-dependent manner, both in the short (P14) [$F_{(2, 28)} = 3.60$, †$p = 0.040$ vs. control] and long term (P70) [$F_{(2, 31)} = 6.43$, ††$p = 0.005$ vs. control] (Fig. 4b). Although hemorrhages were larger in regions closer to the injection site, distant regions were also affected, and hemorrhage burden was increased in the cortex both at P14 [$F_{(2, 63)} = 7.56$, ††$p = 0.040$ vs. control] and P70 [$F_{(2, 60)} = 11.04$, ††$p < 0.001$ vs. control] (Fig. 4c). Contralateral hemispheres were also analyzed and a similar dose-dependent pattern was observed although to a lesser extent (data not shown).

Collagenase-Induced GMH-IVH Provokes a Widespread Inflammatory Response

We analyzed the inflammatory process by measuring microglia burden in the immediate surroundings of the injection site. In the SVZ, we detected a significant increase of microglia burden at P14 [$F_{(2, 298)} = 7.72$, ††$p = 0.001$ vs. control] after collagenase injections, and this effect was still detectable at P70 [$F_{(2, 246)} = 17.66$, **$p < 0.01$ vs. the rest of the groups ††$p = 0.001$ vs. control] (Fig. 4e). A similar profile was observed in the hippocampus, although differences only reached statistical significance in the long term (P14 [$F_{(2, 380)} = 1.28$, $p = 0.465$], P70 [$F_{(2, 298)} = 20.79$, **$p < 0.01$ vs. the rest of the groups, ††$p < 0.01$ vs. control]) (Fig. 4f). Also, regions located further away from the injection sites were affected: an increased microglia burden was observed in the cortex, both in the short and the long term (P14 [$F_{(2, 1852)} = 5.93$, ††$p = 0.003$ vs. control], P70 [$F_{(2, 1544)} = 77.05$, **$p < 0.01$ vs. the rest of the groups, ††$p = 0.003$ vs. control]) (Fig. 4g, h), and to a lesser extent, a similar profile was observed in the contralateral hemispheres (data not shown).

GMH-IVH Induces Tau Hyperphosphorylation in the Long Term

We did not detect any significant changes in tau hyperphosphorylation in the short term, at P14, in any of the regions under study (Fig. 5a): striatum [$F_{(2, 10)} = 1.95$, $p = 0.193$], hippocampus [$F_{(2, 11)} = 0.66$, $p = 0.533$], or cortex [$F_{(2, 10)} = 1.15$, $p = 0.353$] (Fig. 5a). In the long term, at P70, tau hyperphosphorylation was significantly increased in regions surrounding the lesioned areas: striatum [$F_{(2, 11)} = 24.078$, **$p < 0.01$ vs. the rest of the groups] and hippocampus [$F_{(2, 11)} = 7.03$, *$p = 0.011$ vs. the rest of the groups], while differences were not observed in distant regions (cortex [$F_{(2, 10)} = 0.55$, $p = 0.591$]) (Fig. 5b). Figure 5c shows illustrative examples of striatal, hippocampal, and cortical tau phosphorylation at P70 in all groups under study.

Collagenase-Induced GMH-IVH Alters Peripheral Blood Biomarkers of Central Alterations

When we analyzed plasma MMP9 levels in our model, we did not detect any significant differences across groups at P14 [$F_{(2, 40)} = 0.676$], $p = 0.514$ or P70 [$F_{(2, 41)} = 1.16$, $p = 0.321$] (Fig. 6a). However, at P14, MMP9 levels were positively correlated with ventricle size enlargement (Pearson's correlation 0.677*, *$p = 0.032$). UCH-L1 levels were increased at P14 in mice treated with the highest dose of collagenase [$F_{(2, 15)} = 4.161$, †$p = 0.036$ vs. control], while differences were no longer detectable in the long term [$F_{(2, 16)} = 2.38$, $p = 0.124$] (Fig. 6b). On the other hand, plasma gelsolin levels were significantly reduced in collagenase-
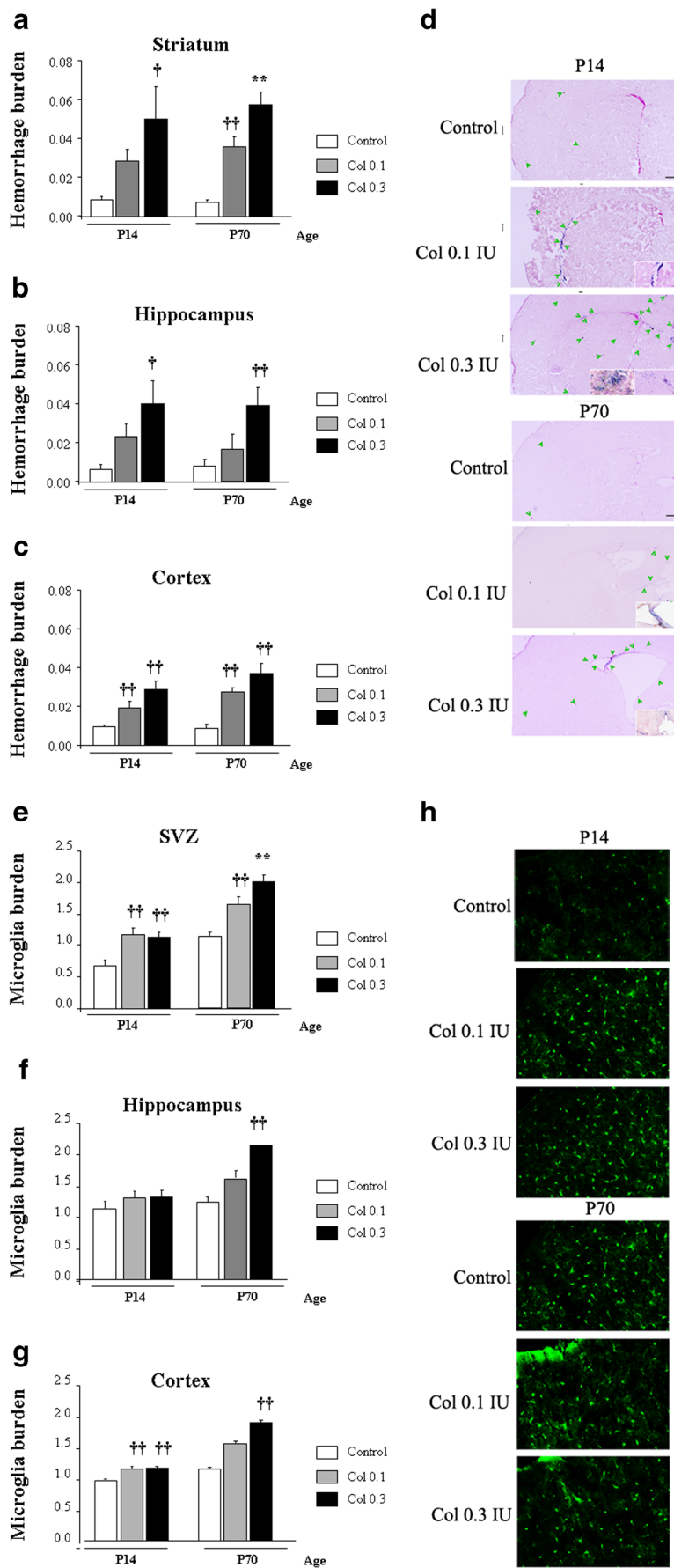
◀ **Fig. 4** Brain hemorrhages and inflammation are increased in the short and the long term after GMH-IVH. **a** Hemorrhage burden was increased in the striatum in the short and the long term after collagenase injections (P14 †$p = 0.046$ vs. control, P70 **$p < 0.01$ vs. the rest of the groups, ††$p < 0.01$ vs. control). **b** Bleeding was also increased in the hippocampus after collagenase lesions (P14 †$p = 0.040$ vs. control, P70 ††$p = 0.005$ vs. control). **c** Hemorrhage burden was also increased in the cortex (P14 †$p = 0.040$ vs. control, P70 ††$p < 0.001$ vs. control). **d** Illustrative example of Prussian blue staining in all groups under study at P14 and P70. *Scale bar* = 250 μm, *inlets* = 50 μm. **e** Microglia burden was increased in the SVZ, surrounding the injection sites (P14 ††$p = 0.001$ vs. control, P70 **$p < 0.01$ vs. the rest of the groups ††$p = 0.001$ vs. control). **f** A similar profile was observed in the hippocampus (P14 $p = 0.465$, P70 **$p < 0.01$ vs. the rest of the groups, ††$p < 0.01$ vs. control). **g** Microglia burden was also increased in the cortex (P14 ††$p = 0.003$ vs. control, P70 **$p < 0.01$ vs. the rest of the groups, ††$p = 0.003$ vs. control). **h** Illustrative example of microglia immunostaining in all groups under study at P14 and P70. *Scale bar* = 50 μm

treated mice at P14 [$F_{(2, 36)} = 10.68$, **$p < 0.01$ vs. control], but differences were no longer detectable in the long term, at p70 [$F_{(2, 41)} = 0.449$, $p = 0.641$] (Fig. 6c). Tau levels in our animal model were significantly increased in a dose-dependent manner at P14 [$F_{(2, 17)} = 9.01$, ††$p = 0.002$ vs. control]. Interestingly, differences were still detectable in the Col 0.3 group at P70 [$F_{(2, 13)} = 5.16$, †$p = 0.022$ vs. control] (Fig. 6d). Significant positive correlations were observed between plasma tau levels and inflammation as measured with microglia burden in the cortex and the SVZ at P14 (Pearson's correlation cortex 0.759*, *$p = 0.01$; SVZ 0.829**, **$p = 0.006$, $n = 9$). Moreover, elevated plasma tau levels in the long term were associated with cognitive impairment in the retention phase of the MWM test (Pearson's correlation −0.541*, *$p = 0.042$, $n = 14$).

GMH-IVH in PTNB Patients Alters Peripheral Blood Biomarkers of Central Alterations

In our human samples from PTNB patients, we detected a similar profile to that observed in our animal model. MMP9 levels were reduced on day 0 and day 7 in PTNB patients with GMH-IVH, although differences did not reach statistical significance ($p = 0.658$ and $p = 0.445$, respectively) (Fig. 6e). UCH-L1 levels were increased immediately after birth in those patients who developed GMH-IVH (*$p = 0.043$ vs. control), while differences were no longer detectable on day 7 ($p = 0.975$) (Fig. 6f). UCH-L1 levels at birth were correlated with hemorrhage severity grade (Spearman's rank correlation 0.574*, *$p = .016$, $n = 17$: 7 control and 10 GMH-IVH). On the other hand, plasma gelsolin levels were significantly reduced at birth in patients who developed GMH-IVH (*$p = 0.046$ vs. control). Gelsolin levels were still reduced 1 week later, although differences did not reach statistical significance ($p = 0.226$) (Fig. 6h). Interestingly, early changes in gelsolin levels (day 0) were negatively correlated with hemorrhage severity grade (Spearman's rank correlation −0.577**, **$p = 0.01$, $n = 19$: 9 control and 11 GMH-IVH).
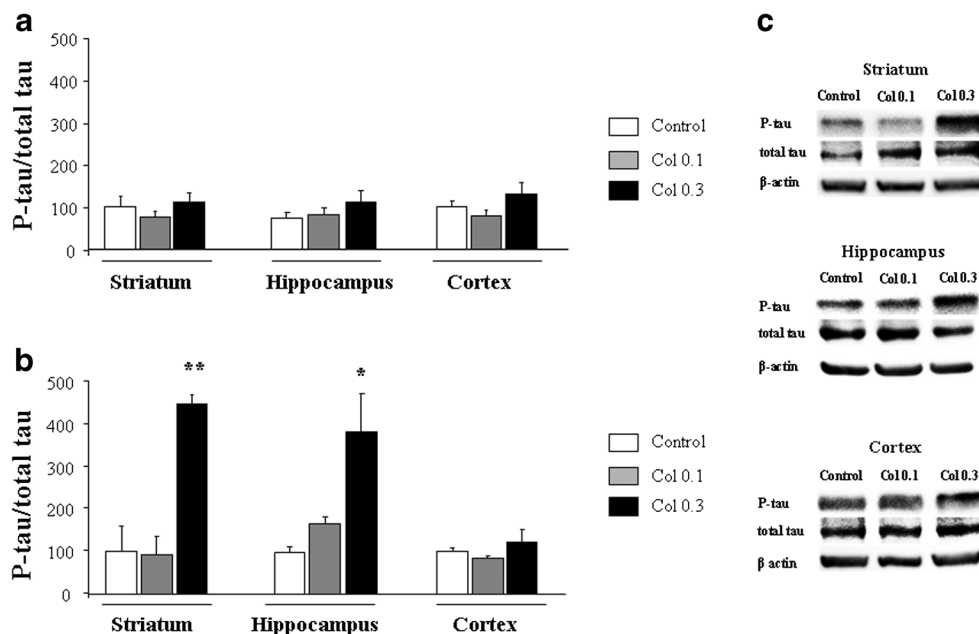

Fig. 5 Increased tau phosphorylation is observed in the long term after GMH-IVH. **a** A slight increase in tau phosphorylation was observed at P14 in animals lesioned with the highest dose of collagenase (0.3 IU), although differences did not reach statistical significance in the striatum ($p = 0.193$), hippocampus ($p = 0.533$), or cortex ($p = 0.353$). **b** In the long term (P70), tau phosphorylation was not significantly affected in the cortex ($p = 0.591$), whereas a significant increase of tau phosphorylation was detected in animals lesioned with collagenase 0.3 IU in the areas surrounding the lesion site: striatum **$p < 0.01$ vs. the rest of the groups and hippocampus *$p = 0.011$ vs. the rest of the groups. **c** Illustrative example of striatal, hippocampal, and cortical tau phosphorylation at P70 in all groups under study
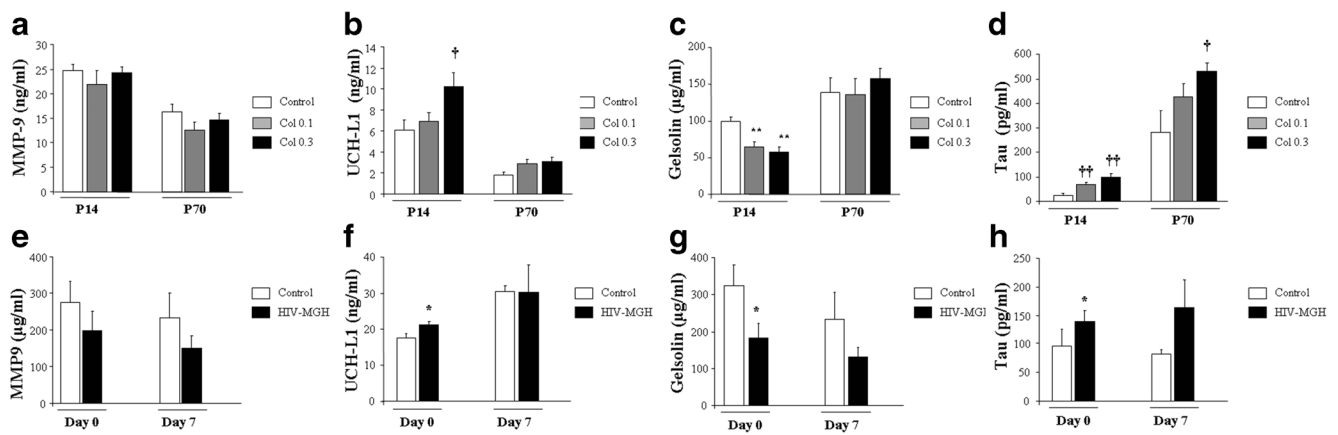
Fig. 6 Peripheral UCH-L1, gelsolin, and tau are altered in collagenase-induced GMH-IVH and in preterm newborns with GMH-IVH. **a** MMP9 levels were not significantly affected in our animal model in the short ($p = 0.514$) or the long term ($p = 0.321$). **b** UCH-L1 levels were increased at P14 in mice with the most severe lesions (†$p = 0.036$ vs. control), and differences did not reach statistical significance in the long term ($p = 0.124$). **c** Gelsolin levels were significantly reduced in collagenase-treated mice at P14 (**$p < 0.01$ vs. control), and no differences were detected at P70 ($p = 0.641$). **d** Tau levels were increased after GMH-IVH at P14 (††$p = 0.002$ vs. control) and at P70 (†$p = 0.022$ vs. control). **e** MMP9 levels were not affected in preterm newborn patients on day 0 or day 7 ($p = 0.658$ and $p = 0.445$, respectively). **f** UHCL-1 levels were increased on day 0 in preterm newborn patients who later developed GMH-IVH (*$p = 0.043$ vs. control), but differences were no longer detectable on day 7 ($p = 0.975$). **g** Gelsolin levels were significantly reduced at birth in patients that would develop GMH-IVH (*$p = 0.046$ vs. control), and while gelsolin levels were still reduced on day 7, differences did not reach statistical significance ($p = 0.226$). **h** Tau levels were significantly higher at birth in preterm newborn patients who later developed GMH-IVH (*$p = 0.046$ vs. control), while differences were no longer detectable on day 7 ($p = 0.161$)

Plasma levels were significantly higher at birth in patients who developed GMH-IVH (*$p = 0.046$ vs. control), while differences were no longer detectable on day 7 ($p = 0.161$) (Fig. 6h). Early changes in tau at birth could not predict GMH-IVH in the newborns; however, 7 days after birth, plasma tau levels were correlated with hemorrhage severity grade (Spearman's rank correlation 0.541*, *$p = 0.03$, $n = 19$: 7 control and 9 GMH-IVH).

Discussion

Short- and long-term neurodevelopmental complications associated with GMH-IVH are a major complication in the PTNB, and information linking pathological features and outcomes are still limited. In order to further explore the mechanisms underlying GMH-IVH, we induced hemorrhages to CD1 newborn mice at ~P7. We chose these mice because the CD1 strains appear to be particularly susceptible to brain injury [19] and this age is commonly used to study similar perinatal scenarios [20]. In our hands, icv administration of collagenase resulted in a dose-dependent cognitive dysfunction that was still detectable in the early adulthood [21] (P70). Previous studies have reported motor activity impairment in collagenase-treated rats at shorter times [9]; however, we did not detect any significant dysfunction in motor activity. It is plausible that different species and assessment times account for these different outcomes. Other studies have reported learning and memory dysfunction in mouse models of neonatal hyperoxia [22]. While our observations are in line with

these studies, to our knowledge, the cognitive performance of this GMH-IVH model has not been tested. In our mouse model, spatial memory was significantly impaired in the MWM task, and a very demanding version of the NOD task [13], assessing "what," "where," and "when" paradigms, also showed a dose-dependent dysfunction in the early adulthood after GMH-IVH induction.

GMH-IVH also resulted in brain atrophy, especially relevant in the long term. Moreover, collagenase lesions also induced a dose-dependent ventricle enlargement both in the short and the long term, in line with previous observations in the plasminogen activator inhibitor 1 knockout mice [23]. We also observed a significant reduction in the number of neurons in the SVZ surrounding the injection site, as previously observed in other models [24]. Interestingly, a similar outcome was observed in areas significantly apart from the SVZ, such as the cortex, suggesting widespread damage after inducing GMH-IVH. These observations are in accordance with previous studies showing that brain injury occurring early during development results in significant and persistent decreases in cortical and hippocampal volumes. Moreover, atrophy of both gray and white matter is also obvious in animal models and human patients with perinatal hypoxic-ischemic encephalopathy [25]. While the underlying cause has not been clarified, this atrophy can be attributed to both loss of infarcted tissue and impaired development of the surrounding tissue over time [20]. On the other hand, since the SVZ is also a main neurogenic niche, we also analyzed

proliferation and neurogenesis in our animal model. The proliferation of neural cells in these zones is pivotal in central nervous system repair: while neurogenesis can occur in response to acute brain injury and neurodegenerative diseases, in the case of GMH-IVH, the age of the animals, the hemorrhage model, and the timing are likely determinants of the outcome of neurogenesis [26, 27]. In our hands, proliferation was not dramatically affected in the short or the long term when we assessed the neurogenic niches. However, neurogenesis was compromised in the SVZ and the DG in the long term after severe lesions were induced (0.3 IU Col), in line with recent observations [28]. Also, studies in preterm infants have reported different patterns of growth impairment depending on the areas affected by hemorrhages, likely explaining different mechanisms through which neurogenesis is disrupted [29]. The type and distribution of human brain lesions differ markedly between developing and mature brains [30], and since collagenase injections were performed in the region under analysis, it is plausible that the local damage was too severe to allow for the recovery of the SVZ. However, while the number of proliferating cells and newly formed neurons is extremely low in regions as the cortex and hippocampus, we observed that both proliferation and neurogenesis were also significantly impaired in our model in these two distant regions. Whereas impaired neurogenesis is unlikely to wholly explain the observed brain atrophy by itself, it may contribute.

The presence of microhemorrhages was increased in a dose-dependent manner in close proximity to the lesions, and to a lesser extent in distant regions. It has been previously hypothesized that structural and functional states of microvessels might account for age-dependent vulnerability [31] and it is possible that the collagenase insult might be enough to induce sparse vascular damage. In line with these observations, we also observed a dose-dependent inflammatory response that was more severe in the areas surrounding the ventricles, as previously described in other models [24]. However, we detected a more widespread inflammatory process in collagenase-treated mice. These observations are in line with previous studies showing an increased number of microglial cells in the brains from GMH-IVH patients, which reaches statistical significance in the SVZ [32].

We also analyzed brain tau levels after GMH-IVH as a marker of neuronal injury. Long-term increased expression was observed in the areas surrounding the lesion sites. To our knowledge, tau has not been previously explored after GMH-IVH in animal models or patients, even though hyperphosphorylated tau exerts toxic effects and is a pathological hallmark of neurodegenerative disorders. In this regard, the presence of hemorrhages and associated ischemic injury could explain the increase in tau phosphorylation, as previously observed in other models with central hemorrhages [17, 33, 34].

We observed a similar profile when we analyzed the peripheral blood in mice and PTNB patients with GMH-IVH. Surprisingly, MMP9 levels were not altered in any of the groups under study. Although previous studies have reported increased MMP9 activity in the rat neonatal brain after ischemic lesions [35] and in plasma from PTNB with IVH [36], actual MMP9 levels have not been assessed, and we cannot exclude that MMP9 activity is affected in our mouse model and GMH-IVH PTNB. However, in mice, we observed that MMP9 levels were significantly correlated with ventricle enlargement, in line with previous observations in CSF from patients [37]. On the other hand, plasma UCH-L1 levels were increased at birth in patients developing GMH-IVH and in our animal model. Although high serum UHCL-1 levels have been reported in other neonatal complications [38], we believe that UHCL-1 levels have not been assessed in preterm newborns who would develop GMH-IVH. Plasma gelsolin levels have been reported to be lower in PTNB with respiratory distress syndrome and those who developed sepsis [39]. It has also been suggested as a putative biomarker of cerebral hemorrhage-related complications in the adult [40]; however, to our knowledge, this is the first approach in which lower gelsolin levels are detected at birth in preterm newborns, who went on later to develop GMH-IVH. Moreover, UCH-L1 and gelsolin levels at birth were correlated with hemorrhage severity grade, supporting their role not only as a prognostic biomarker but also as promising predictors of GMH-IVH. Similarly, to our knowledge, this is the first time that plasma tau levels have been measured in preterm infants. Plasma tau levels were altered in patients with GMH-IVH, and on day 7 after birth, hyperphosphorylated tau levels were correlated with hemorrhage severity grade, indicating this protein may be a potential biomarker of brain damage in GMH-IVH.

Altogether, we characterized a new animal model of GMH-IVH, in the short and the long term, that resembles neurodevelopmental and morphopathological features observed in preterm newborn patients with this dreaded complication of prematurity. This animal model exhibited learning and memory deficits, brain atrophy, or impaired neurogenesis. We also observed widespread bleeding and inflammation in the immature brain after GMH-IVH induction and altered levels of classical biomarkers of neuronal injury, such as phospho-tau. Moreover, determination of widely available peripheral blood biomarkers in both our animal model and patients revealed that altered UCH-L1 and gelsolin levels at birth might predict the future development and severity of GMH-IVH in preterm newborns. These biomarkers could also help to identify and select at-risk newborns for a closer monitoring by neuroimaging approaches or for early neurosurgery.

Compliance with Ethical Standards

Conflict of Interest The authors declare that they have no conflict of interest.

References

1. Mukerji A, Shah V, Shah PS (2015) Periventricular/intraventricular hemorrhage and neurodevelopmental outcomes: a meta-analysis. Pediatrics 136(6):1132–1143

2. Tabata H, Yoshinaga S, Nakajima K (2012) Cytoarchitecture of mouse and human subventricular zone in developing cerebral neocortex. Exp Brain Res 216(2):161–168

3. de Vries LS, Benders MJ, Groenendaal F (2015) Progress in neonatal neurology with a focus on neuroimaging in the preterm infant. Neuropediatrics 46(4):234–241

4. Adams-Chapman I (2009) Insults to the developing brain and impact on neurodevelopmental outcome. J Commun Disord 42(4):256–262

5. Adams-Chapman I, Hansen NI, Stoll BJ, Higgins R (2008) Neurodevelopmental outcome of extremely low birth weight infants with posthemorrhagic hydrocephalus requiring shunt insertion. Pediatrics 121(5):e1167–e1177

6. Bolisetty S, Dhawan A, Abdel-Latif M et al (2014) Intraventricular hemorrhage and neurodevelopmental outcomes in extreme preterm infants. Pediatrics 133(1):55–62

7. Patra K, Wilson-Costello D, Taylor HG, Mercuri-Minich N, Hack M (2006) Grades I–II intraventricular hemorrhage in extremely low birth weight infants: effects on neurodevelopment. J Pediatr 149(2):169–173

8. Brouwer AJ, Groenendaal F, Benders MJ, de Vries LS (2014) Early and late complications of germinal matrix-intraventricular haemorrhage in the preterm infant: what is new? Neonatology 106(4):296–303

9. Alles YC, Greggio S, Alles RM et al (2010) A novel preclinical rodent model of collagenase-induced germinal matrix/intraventricular hemorrhage. Brain Res 1356:130–138

10. Balasubramaniam J, Del Bigio MR (2006) Animal models of germinal matrix hemorrhage. J Child Neurol 21(5):365–371

11. Lekic T, Manaenko A, Rolland W et al (2012) Rodent neonatal germinal matrix hemorrhage mimics the human brain injury, neurological consequences, and post-hemorrhagic hydrocephalus. Exp Neurol 236(1):69–78

12. Abbadie C, Lindia JA, Cumiskey AM et al (2003) Impaired neuropathic pain responses in mice lacking the chemokine receptor CCR2. Proc Natl Acad Sci U S A 100(13):7947–7952

13. Ramos-Rodriguez JJ, Ortiz O, Jimenez-Palomares M et al (2013) Differential central pathology and cognitive impairment in prediabetic and diabetic mice. Psychoneuroendocrinology 38(11):2462–2475

14. Ramos-Rodriguez JJ, Molina-Gil S, Ortiz-Barajas O et al (2014) Central proliferation and neurogenesis is impaired in type 2 diabetes and prediabetes animal models. PLoS One 9(2):e89229

15. Infante-Garcia C, Jose Ramos-Rodriguez J, Marin-Zambrana Y et al (2017) Mango leaf extract improves central pathology and cognitive impairment in a type 2 diabetes mouse model. Brain Pathol 27:449–507

16. Ramos-Rodriguez JJ, Spires-Jones T, Pooler AM et al (2016) Progressive neuronal pathology and synaptic loss induced by prediabetes and type 2 diabetes in a mouse model of Alzheimer's disease. Mol Neurobiol 54:3428–3438

17. Infante-Garcia C, Ramos-Rodriguez JJ, Galindo-Gonzalez L, Garcia-Alloza M (2016) Long-term central pathology and cognitive impairment are exacerbated in a mixed model of Alzheimer's disease and type 2 diabetes. Psychoneuroendocrinology 65:15–25

18. Ramos-Rodriguez JJ, Infante-Garcia C, Galindo-Gonzalez L et al (2015) Increased spontaneous central bleeding and cognition impairment in APP/PS1 mice with poorly controlled diabetes mellitus. Mol Neurobiol 53:2685–2697

19. Sheldon RA, Sedik C, Ferriero DM (1998) Strain-related brain injury in neonatal mice subjected to hypoxia-ischemia. Brain Res 810(1–2):114–122

20. Semple BD, Blomgren K, Gimlin K, Ferriero DM, Noble-Haeusslein LJ (2013) Brain development in rodents and humans: identifying benchmarks of maturation and vulnerability to injury across species. Prog Neurobiol 106–107:1–16

21. Dutta S, Sengupta P (2016) Men and mice: relating their ages. Life Sci 152:244–248

22. Ramani M, van Groen T, Kadish I, Bulger A, Ambalavanan N (2013) Neurodevelopmental impairment following neonatal hyperoxia in the mouse. Neurobiol Dis 50:69–75

23. Leroux P, Omouendze PL, Roy V et al (2014) Age-dependent neonatal intracerebral hemorrhage in plasminogen activator inhibitor 1 knockout mice. J Neuropathol Exp Neurol 73(5):387–402

24. Georgiadis P, Xu H, Chua C et al (2008) Characterization of acute brain injuries and neurobehavioral profiles in a rabbit model of germinal matrix hemorrhage. Stroke 39(12):3378–3388

25. Brouwer MJ, de Vries LS, Kersbergen KJ et al (2016) Effects of posthemorrhagic ventricular dilatation in the preterm infant on brain volumes and white matter diffusion variables at term-equivalent age. J Pediatr 168:41–49e1

26. Mino M, Kamii H, Fujimura M et al (2003) Temporal changes of neurogenesis in the mouse hippocampus after experimental subarachnoid hemorrhage. Neurol Res 25(8):839–845

27. Otero L, Zurita M, Bonilla C et al (2012) Endogenous neurogenesis after intracerebral hemorrhage. Histol Histopathol 27(3):303–315

28. Tang J, Miao H, Jiang B et al (2017) A selective CB2R agonist (JWH133) restores neuronal circuit after germinal matrix hemorrhage in the preterm via CX3CR1+ microglia. Neuropharmacology 119:157–169

29. Kim H, Gano D, Ho ML et al (2016) Hindbrain regional growth in preterm newborns and its impairment in relation to brain injury. Hum Brain Mapp 37(2):678–688

30. Miller SP, Ferriero DM (2009) From selective vulnerability to connectivity: insights from newborn brain imaging. Trends Neurosci 32(9):496–505

31. Porte B, Hardouin J, Zerdoumi Y et al (2017) Major remodeling of brain microvessels during neonatal period in the mouse: a proteomic and transcriptomic study. J Cereb Blood Flow Metab 37(2):495–513

32. Supramaniam V, Vontell R, Srinivasan L et al (2013) Microglia activation in the extremely preterm human brain. Pediatr Res 73(3):301–309

33. Wen Y, Yang S, Liu R et al (2004) Transient cerebral ischemia induces aberrant neuronal cell cycle re-entry and Alzheimer's disease-like tauopathy in female rats. J Biol Chem 279(21): 22684–22692

34. Zhang Q, Gao T, Luo Y et al (2012) Transient focal cerebral ischemia/reperfusion induces early and chronic axonal changes in rats: its importance for the risk of Alzheimer's disease. PLoS One 7(3):e33722

35. Ranasinghe HS, Williams CE, Christophidis LJ et al (2009) Proteolytic activity during cortical development is distinct from that involved in hypoxic ischemic injury. Neuroscience 158(2):732–744

36. Schulz CG, Sawicki G, Lemke RP et al (2004) MMP-2 and MMP-9 and their tissue inhibitors in the plasma of preterm and term neonates. Pediatr Res 55(5):794–801

37. Okamoto T, Takahashi S, Nakamura E et al (2010) Increased expression of matrix metalloproteinase-9 and hepatocyte growth factor in the cerebrospinal fluid of infants with posthemorrhagic hydrocephalus. Early Hum Dev 86(4):251–254

38. Douglas-Escobar M, Yang C, Bennett J et al (2010) A pilot study of novel biomarkers in neonates with hypoxic-ischemic encephalopathy. Pediatr Res 68(6):531–536

39. Kose M, Elmas T, Gokahmetoglu S et al (2014) Predictive value of gelsolin for the outcomes of preterm neonates: a pilot study. Pediatr Int 56(6):856–859

40. Chou SH1, Lee PS, Konigsberg RG et al (2011) Plasma-type gelsolin is decreased in human blood and cerebrospinal fluid after subarachnoid hemorrhage. Stroke 42(12):3624–3627